Performance predictions in solid oxide fuel cells

Lin, Yongming; Beale, Steven

Publisher's version / Version de l'éditeur:
https://doi.org/10.1016/j.apm.2006.03.009
Applied Mathematical Modelling, 30, 2006

Available online at www.sciencedirect.com
SCIENCE DIRECT®
Applied Mathematical Modelling 30 (2006) 1485–1496
APPLIED MATHEMATICAL MODELLING
www.elsevier.com/locate/apm

Performance predictions in solid oxide fuel cells

Y. Lin, S.B. Beale *

National Research Council, Montreal Road, Ottawa, Ont., Canada K1A 0R6

Received 30 April 2005; accepted 7 October 2005
Available online 27 April 2006

Abstract

The results of numerical calculations performed for planar solid oxide fuel cells are presented. Two different approaches are developed: (i) A detail numerical method and (ii) a presumed flow method. In the first approach, a commercial computational fluid dynamics code is employed, and user-defined-functions are developed to account for electro-chemical considerations. In the second approach, where the momentum equations do not require to be solved, an in-house code is developed and used to perform calculations. In both cases the following coupled physicochemical phenomena are modelled; heat and mass transfer, electrochemistry and electric potential. The polarisation curve is generally accepted as an important performance measure of the fuel cell. Performance predictions for this characteristic made by the two different approaches are compared. Results show voltage losses due activation, Ohmic resistance, and mass transfer in a typical solid oxide fuel cell, over a range of current density values. The results for the detailed numerical method are discussed in some detail with regard to the influence of different parameters on the overall performance of the device.

1. Introduction

Fuel cells combine hydrogen-rich fuel with oxygen to generate electricity, water, and heat. The fuel cell was invented by Grove in 1839, and the first alkaline fuel cell prototype developed by Bacon in 1932, see Berger [1]. High energy efficiency and environmentally benign attributes make the fuel cell a candidate for future power sources. In the last two decades, commercialization of fuel cells has become important, with the associated development of new technologies to overcome the major engineering and cost barriers for this technology.

These developments have stimulated progress in fuel cell modelling and numerical analysis: Computational fluid dynamics (CFD) is playing an important role in assisting fuel cell manufacturers design products, and speeding up the development process. The solid oxide fuel cell (SOFC) operates at 800–1000 °C and is considered a potential source of electricity for stationary and other applications. The solid-state electrolyte is made from zirconia, a brittle material, which is liable to crack under sufficient stress. SOFCs are typically operated in stacks in order to increase the overall voltage of the unit.

* Corresponding author. Tel.: +1 613 993 3487; fax: +1 613 941 1571.
E-mail address: steven.beale@nrc-cnrc.gc.ca (S.B. Beale).

0307-904X/$ - see front matter
doi:10.1016/j.apm.2006.03.009

Nomenclature

A	area, m^2
c_p	specific heat, J/kg K
C	molar concentration, mol/m^3
D	diffusion coefficient, m^2/s
E	Nernst potential, V, activation energy, J/mol
F	Faraday's constant, 96,485.3, Coulomb/mol
G	Gibb's free energy of formation, J/mol
H	enthalpy of formation, J/mol
i''	current density, A/m^2
k	permeability, m^2
M	molecular weight
m	mass fraction
n	number of electrons, normal direction
P	power density, W/m^2
p	pressure, Pa
R	resistance, Ω, gas constant, 8.3144×10^3, J/mol
S	source term
T	temperature, °C or K
U	superficial velocity, m/s
u	velocity, interstitial velocity, m/s
V	cell voltage, V
V	volume, m^3
x	molar fraction

Greek symbols

α	transfer coefficient, heat transfer coefficient, W/m^2 K
β	coefficient, S/m
ε	porosity
Φ	electric field potential, V
Γ	exchange coefficient, kg/ms
η	overpotential, V
μ	dynamic viscosity, kg/m s
ρ	gaseous mixture density, kg/m^3
σ	electrical conductivity, S/m
τ	tortuosity

Superscripts

0	reference value
$''$	per unit area
$'''$	per unit volume

Subscripts

a	anode
c	cathode
e	electrolyte

Numerical simulation tools are used to simulate the distributions of temperature and thermally-induced stresses, to ensure the integrity of the SOFC design, and to predict the overall performance of the device.

Techniques have advanced significantly since publication of pioneering works such as Vayenas et al. [2]. Both micro-scale and macro-scale models may be found. Microscopic models are aimed at building better electrodes and electrolytes, whereas macroscopic models generally target cell and stack optimization. Reviews of modern modelling methods for SOFCs may be found in [3,4].

The physicochemical transport phenomena (and the corresponding mathematical models used to describe those phenomena) associated with fuel cells are complex. These include; mass transfer of multi-species gas mixtures in micro-channels and porous diffusion layers, sources of heat, mass and species due to electrochemical reactions, and the impact of local current density on kinetic charge transfer and other voltage losses. Ideally, numerical calculations would reproduce all the above mentioned phenomena faithfully. Such a scheme is detailed below and referred-to as detailed a numerical method (DNM). This approach, however, requires computer resources which are not generally available when considering practical engineering designs, and mesh-independent results may not be feasible for large-scale designs, at least for the time-being.

To alleviate this, simplified models have also been developed. Beale et al. [5,6] proposed two alternative possibilities, a CFD-based distributed resistance analogy (DRA) and a non-CFD based presumed (upstream) flow method (PFM). Both avoid the necessity for employing fine meshes, by assuming momentum/heat and mass transfer may be estimated by introducing appropriate drag, and heat and mass transfer coefficients. These simplified approaches have been verified and proven to be realistic alternatives to more detailed CFD simulations. In this paper further progress to both detailed and simplified transport models are presented, compared and discussed. User-defined-codes must be developed and implemented to perform detailed numerical calculations for fuel cells. These require that a large parallel computer cluster be available for use. The main advantage of performing such calculations is that the fine details of the multi-species gas flow in the channels, mass transfer in the porous gas diffusion layers (GDLs), and local distributions of electric potential and current density may be captured. When coarse-grid approaches (whether CFD-based or otherwise) are employed, mass transfer and electric potential are not computed whole-field, but modelled using algebraic relationships. In previous studies, it was found that even though the PFM uses only a small fraction of the computational resources required for a DNM, it does nonetheless provide good performance predictions for SOFCs. The PFM developed for this programme of research differs from [5,6] in that a body-fitted grid corresponding to the solid–fluid walls was constructed; whereas previously, local volume-averaging resulted in the distinction between solid and fluid zones being blurred.

In the present study, the electric potential and local current distribution within a SOFC are analysed using the detailed analysis, and the importance of this together with the effect of oxygen concentration upon performance is discussed. It is shown that for the anode supported SOFC type, where the GDL is relatively thin; uneven current density distribution is very likely across the electrolyte–cathode interface, due to the impact of oxygen diffusion and the current distribution within the GDL.

2. Model description

The geometry of the SOFC considered in this study is shown in Fig. 1. The basic unit is composed of seven (7) layers in the vertical direction (from bottom-to-top): (1) air-side interconnect, (2) air-side gas channels, (3) porous cathode, (4) electrolyte, (5) porous anode, (6) fuel-side gas channels, and (7) interconnect on fuel side. The dimensions of the layers are shown in Table 1. The flow channels are embedded within the interconnects in the form of micro-channels, of rectangular cross-section. The metallic interconnects also function as electrical connectors when current is flowing through the SOFC. The fuel and air channels are separated by GDLs and by the electrolyte layer. As shown, the fluids are in cross-flow. Both air and fuel are introduced to the fuel cell via manifolds (not shown).

The physical–chemical transport phenomena in a SOFC are strongly coupled. For convenience, we classify them into the following categories: (i) mass transfer in gas channels and porous media; (ii) heat transfer in all constituent materials; (iii) electrochemical reactions at interfaces between electrolyte and electrodes; (iv) electronic and ionic charge transfer through solid and porous media.

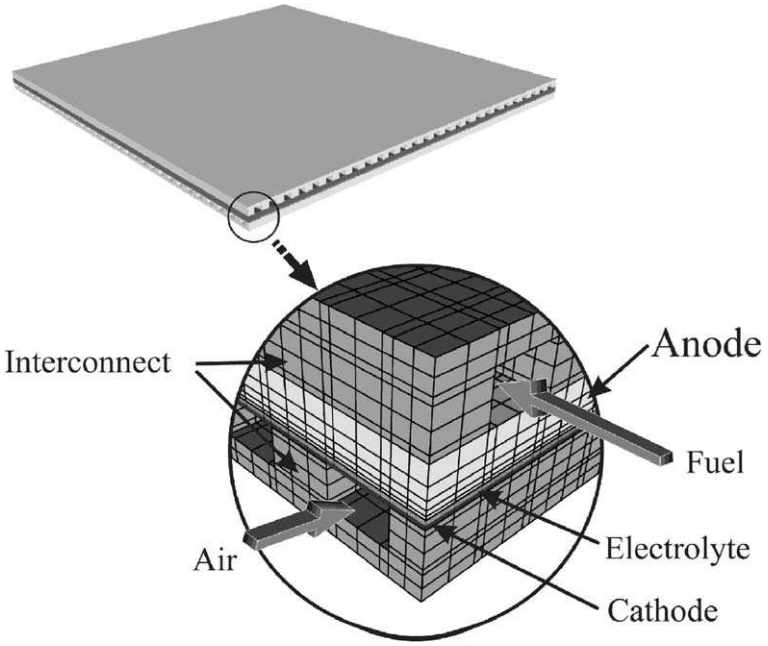

Fig. 1. SOFC geometry, showing meshing details.

Table 1
Physical properties of materials in SOFC

	Thickness (mm)	Electrical conductivity (S/m)	Thermal conductivity (W/m K)
Anode	0.1	10^5	11
Electrolyte	0.1	Fig. 2	2.7
Cathode	1.0	7690	2
Interconnect	1.143	200	2

2.1. Mass transfer

Mass transfer plays an important role in the gas micro-channels. The steady-state species conservation equation is

$$\mathrm{div}(\rho u m_i) - \mathrm{div}(\Gamma \mathrm{grad}\ m_i) = S_i''', \tag{1}$$

where ρ is the mixture density, m_i is mass fraction of species i, u is local velocity, Γ is the exchange coefficient, and S_i''' is a volumetric source term. Darcy's law is considered to apply within the porous electrodes,

$$U = \varepsilon u = -\frac{k}{\mu}\mathrm{grad}\ p, \tag{2}$$

where u is a local pore or interstitial velocity, U is a filter or superficial velocity, k is permeability, ε porosity, and μ viscosity.

Mass transfer in the GDL may be written in the same form as Eq. (1), but based on an effective exchange coefficient Γ_{eff}, defined by

$$\Gamma_{\mathrm{eff}} = \Gamma \frac{\varepsilon}{\tau^2}, \tag{3}$$

where τ is referred to as a tortuosity. Air and fuel are composed of multiple species, and their mass diffusion coefficients, mixture viscosity, and thermal conductivity are computed based on effective values [7]. At the interface between the porous electrodes and the electrolyte, the source term per unit area, S'', for any given species (reactant/product) may be written,

$$S'' = \pm\frac{M}{nF}i'', \tag{4}$$

where M is molecular weight, n the number of electrons involved in the electrochemical reaction, F is Faraday's constant and i'' is the local current density at the interface. The above formulation is sufficient for the DNM used to generate the results in this paper.

Further additional simplifications must be made in a PFM: It is assumed that the flow in the gas micro-channels is fully-developed, and that the drag coefficient is known. One side of each channel is a porous wall and mass transfer (injection or suction) occurs, so the velocity profile will be asymmetric [8,9]. The impact of this upon mass transfer is discussed in [10]. For the present study, a constant value of Sherwood number based on fully-developed duct flow, assuming negligibly small mass transfer was presumed [11]. Similar assumptions were made for mass transfer in the GDLs.

2.2. Heat transfer

Convective heat transfer is the dominant transfer mechanism in the micro-channels, while conduction governs the heat flux in solid materials, such as the current-collecting interconnects, porous electrodes and electrolyte, i.e. the problem is one of conjugate heat transfer, through multiple layers of materials, both fluid and solid.

Consider the reaction

$$\mathrm{H_2} + \frac{1}{2}\mathrm{O_2} \rightarrow \mathrm{H_2O}. \tag{5}$$

From a thermodynamic point-of-view, the available thermal energy resulting from the chemical reaction is the enthalpy of formation, ΔH, whereas the available electrical energy is the Gibb's energy of formation, ΔG. The difference must either be converted to, or provided as heat. For the hydrogen reaction, above, $\Delta H < \Delta G$, and hence the electro-chemical reaction is exothermic. The entropy of formation, under ideal circumstances, is just $(\Delta H - \Delta G)/T$.

In reality, owing to irreversible electrical (Ohmic) and kinetic (activation) terms, additional chemical energy is converted into heat, not electricity. Thus if V is the operating voltage of the fuel cell, then the overall heat source per unit area may be written as,

$$S'' = \left(\frac{\Delta H}{nF} - V\right)i'', \tag{6}$$

where i'' is the local current density. Eq. (6) is an expression for the heat generated due to all sources.

The principle of conservation of energy within the flow channels is governed by the following equation, for steady-state,

$$\mathrm{div}(\rho u c_p T) - \mathrm{div}(k\ \mathrm{grad}\ T) = S''', \tag{7}$$

where T is temperature, k is thermal conductivity, c_p is specific heat, and S''' is the volumetric rate of heat generation. Heat conduction through the solid regions can be expressed as

$$\mathrm{div}\ (k\ \mathrm{grad}\ T) + S''' = 0. \tag{8}$$

In the PFM the diffusion terms are replaced by rate equations, at the wall, namely

$$-k\left.\frac{\mathrm{d}T}{\mathrm{d}n}\right|_{\mathrm{w}} = \alpha\Delta T, \tag{9}$$

where α is a heat transfer coefficient (the symbol h is also frequently encountered). The convective heat transfer is thus obtained from a Nusselt number correlation for the duct geometry [11], and not by the performance of

detailed calculations using a fine mesh concentrated near the wall region. Thus both mesh size and run time are reduced substantially. Thermal radiation was not considered in this study.

Heat is generated by three mechanisms: (i) The electrochemical half-reactions generate heat in the two electrodes as previously discussed (ii) Joule heating occurs in the electrolyte, electrodes, and interconnects, due to the resistance to migration of oxygen ions and electrons, (iii) heat dissipation in the electrodes results from activation overpotentials (charge transfer effects) discussed below. Thus for a control volume ΔV in contact with a reaction area ΔA, the total heat source may be conveniently summarised as follows:

$$S = \left(\frac{\Delta H - \Delta G}{T}\right)\Delta A + \sigma(\nabla \Phi)^2 \Delta V + i'' \eta \Delta A, \tag{10}$$

where σ is electrical conductivity, Φ is the electric field potential, and η is the activation overpotential, defined below. The reader will note that there are both ionic and electronic potentials in the electrolyte and interconnects, respectively (both potentials may be present in the active region of the electrodes). In this study, the electronic potential is solved-for whole field, whereas the ionic potential is treated algebraically.

2.3. Electrochemistry

Eq. (5) may be written in terms of two half-reactions at the electrodes,

$$\frac{1}{2}O_2 + 2e^- \rightarrow O^{2-} \tag{11}$$

$$H_2 + O^{2-} \rightarrow H_2O + 2e^- \tag{12}$$

The first reaction is endothermic and the second exothermic. The half-reactions take place on either side of the electrolyte, which is very thin, and hence it is appropriate to treat the two together. The Nernst potential may be written as follows:

$$E = E^0 + \frac{RT}{2F} \ln\left(\frac{x_{H_2} x_{O_2}^{1/2}}{x_{H_2O}}\right) + \frac{RT}{4F} \ln P_a, \tag{13}$$

where x is mole fraction, and E^0 is a reference potential. Eq. (13) determines the thermodynamically maximum possible cell voltage. However, when a small current, δi, flows, there is a corresponding reduction in the cell voltage, $\eta = \delta V$. This is due to activation losses at the electrodes. The activation overpotential is commonly written as a function of current density, $\eta(i'')$, in the following implicit form:

$$i'' = i_0''\left\{\exp\left(\alpha_a \frac{F}{RT}\eta\right) - \exp\left(-\alpha_c \frac{F}{RT}\eta\right)\right\}, \tag{14}$$

where α_a and α_c are referred to as anodic and cathodic transfer coefficients, and i_0'' is an exchange current density. Eq. (14) is referred to as a Butler–Volmer equation. There are two such terms; for the anode and the cathode. However in a SOFC, anode losses are generally small in comparison to those at the cathode. The dependence of the exchange current density on species concentration was presumed to follow the expressions given by Costamagna et al. [12].

2.4. Electric potential

Electronic conduction occurs in the relatively thick metallic interconnects, and the porous electrodes. Charge transport is governed by a Laplace equation

$$\mathrm{div}(\sigma\ \mathrm{grad}\ \Phi) = 0. \tag{15}$$

The local current density vector may be computed according as

$$i'' = -\sigma\ \mathrm{grad}\ \Phi. \tag{16}$$

In the present study, it is tacitly assumed only ions and not electrons flow through the electrolyte. Since the electrolyte is very thin, a locally one-dimensional (1-D) approach is considered appropriate for computing the

potential in the ionic-conducting electrolyte layer. The electrodes are thus taken to be perfect electrical conductors, so the potential across the electrode–electrolyte interface is constant.

The cell voltage, V, may be expressed as

$$V = E - \eta_a - \eta_c - \sum_k i'' R_k, \tag{17}$$

where η_a and η_c are the activation overpotentials on the anode and cathode sides, and $\sum i'' R_k$ is the sum of all resistive losses; ionic (electrolyte) and electronic (interconnects, electrodes), and R_k are the corresponding resistance values. Similarly the voltage across the anode–cathode-electrolyte assembly (excluding the interconnect) may be written as $V_{ac} = E - \eta_a - \eta_c - i'' R_e$, provided the resistances of the anode and cathode are small in comparison to that of the electrolyte. The assumption of a thin electrolyte is equivalent to postulating that the electrolyte current flows in a 1-D direction and that the potential difference between the electrodes is locally constant.

Two different types of boundary conditions are encountered: (a) galvanostatic conditions, where the mean current density $\bar{i}''$ (or just the current, i) is presumed known; or (b) potentiostatic conditions where it is the cell voltage, V, which is prescribed. The former are assumed here. It is therefore required that the cell potential across the anode–cathode assembly be computed. This is readily obtained as

$$V_{ac} = \frac{\overline{V^*_{ac}/R_e} - \bar{i}''}{\overline{1/R_e}}, \tag{18}$$

where V^*_{ac} is the value at the present iteration, and $\bar{i}''$ is the prescribed mean current density, and the overbars denote spatially-averaged values.

At the anode and cathode interfaces, it is presumed that,

$$-\sigma \frac{\partial \Phi}{\partial n}\bigg|_a = -\sigma \frac{\partial \Phi}{\partial n}\bigg|_c = i''|_e, \tag{19}$$

i.e. a 3-D simulation is performed within the interconnect material, but a 1-D potential calculation is considered sufficient for the electrode–electrolyte assembly.

The electrical conductivity of the electrolyte strongly depends on the temperature. This is computed, using the correlation of Nagata et al. [13] as follows:

$$\sigma = \beta_1 \exp(-\beta_2/T), \tag{20}$$

where $\beta_1 = 3.34 \times 10^4$ S/m and $\beta_2 = 1.03 \times 10^4$ K. Fig. 2 shows the electrical conductivity of the electrolyte as a function of temperature. The electrical conductivity of all other layers is assumed constant. These are provided in Table 1.

2.5. Numerical methods

The physicochemical hydrodynamics were incorporated into both a DNM and a PFM. The implementation is as follows (precise details vary depending as to which procedure was adopted): In both cases a 3-D rectilinear mesh was constructed which passed through all solid and fluid regions. The meshes were body-fitted, in the sense that the boundaries between different materials (fuel, air, interconnects etc.) corresponded to the surface of the mesh cells, see Fig. 1. For the DNM, a total mesh size of 483,936 compute cells was employed. For the DNM, the mesh is concentrated in the near wall region to capture local variations in the velocity gradient. For the PFM the total number of cells was 11,767. Thus the advantage of using estimated values for Sherwood and Nusselt numbers in the PFM is manifested by a reduction in mesh size by a factor of 40 or more.

The DNM was implemented by means of a commercial CFD code, Fluent, which is based on a finite-volume method. This code was used to perform all fluid flow, heat, mass fraction, and potential calculations. Field variables were stored at the centres of the grid cells. The pressure-corrected momentum equations were solved based on a co-located scheme for velocity. Harmonic averaging was employed when computing the linear coefficients in the finite-volume equations. The electric, electrochemical and other models specific to SOFCs described in detail above, were all implemented by means of user-defined-functions developed and

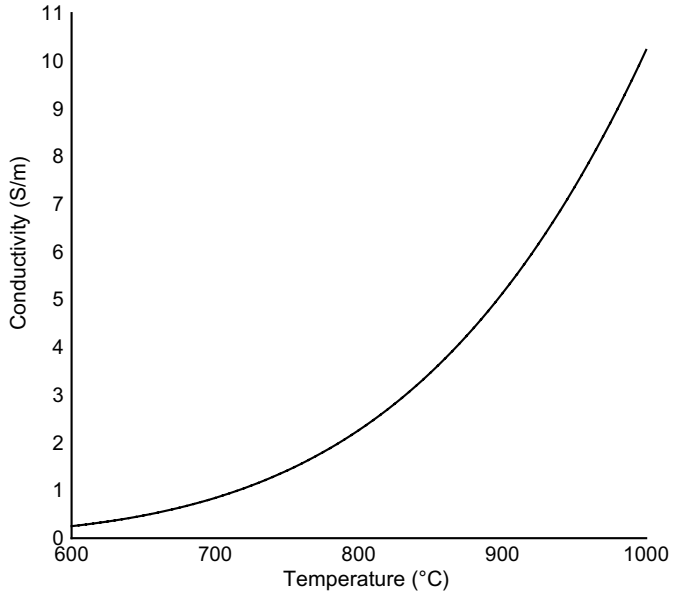

Fig. 2. Electrolyte conductivity of zirconia (S/m) as a function of temperature.

coded in-house. In this manner, physical properties, source terms, and electric field boundary conditions etc. were all set at run-time.

The solution algorithm proceeded as follows:

1. Define solid, fluid and porous-media regions, assign physical properties, and prescribe boundary conditions. Initialise all state-variables.
2. Solve system of transport equations.
3. Calculate Nernst potential, overpotential, electrolyte conductivity.
4. Calculate cell voltage.
5. Calculate source terms for species, mass, enthalpy and potential.
6. Repeat steps (2)–(5).

For the PFM, an in-house code based on the assumption that the flow at the inlets to the fuel cell is known and constant, was developed. Since, a fully-developed velocity profile is presumed; a solution of the momentum and pressure-correction equations is not required. Local bulk velocities are obtained from the continuity equation based on upstream values and known electrochemical sources and sinks, obtained from Eq. (4). Species mass fractions are handled in a similar manner. Because of the elliptic nature of heat conduction, Eq. (8), the energy equation was solved-for with a 3-D finite-difference scheme. The electric potential was treated in a similar manner. Fluid–solid heat transfer was computed using the rate equation, Eq. (9), based on a Nusselt number correlation for fully-developed heat transfer. Wall mass fractions are required in the Nernst and Butler–Volmer equations. These were computed from bulk values, by means of a Sherwood number correlation for fully-developed mass transfer. A generalised minimum residual algorithm [14] was employed to obtain the iterative solution to the energy and electric potential equations.

3. Results and discussion

3.1. SOFC performance predictions

The polarisation curve provides a convenient snapshot of the performance of a fuel cell. Fig. 3 is an example of this performance measure. Cell voltage, V, is given as a function of average current density, $\bar{i}''$. The

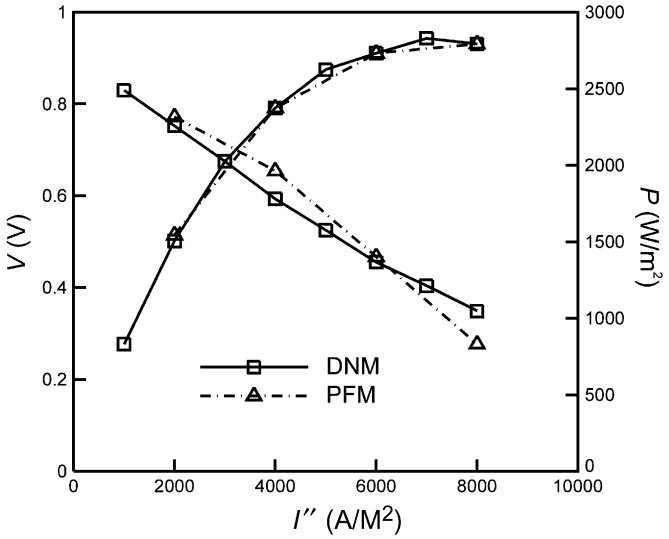

Fig. 3. Polarisation curve.

polarisation curve is not unique for any given SOFC unit under all operating conditions; rather it varies with operating parameters such as the chemical components of the fuel and oxidant, utilization rates for air and fuel, operating temperature, etc. The polarisation curve shown in Fig. 3 is for 50% utilization rate for hydrogen and 25% for oxygen. Results obtained for both the CFD-based DNM code and the simplified PFM code are displayed.

Associated with the typical polarisation curve are three distinct zones: At low current density, the potential is reduced by activation or charge transfer losses; Ohmic losses generally occur at intermediate current density, and concentration (mass transfer) losses may reduce the voltage at high $\bar{i}''$. It can be seen from Eq. (14), that losses due to activation will be minimal at high temperatures, i.e., the voltage losses due to activation are not as significant in high temperature SOFCs as in other low temperature fuel cells, such as proton exchange membrane fuel cells. For the present case, a large part of the V–$\bar{i}''$ curve is dominated by Ohmic losses. Optimum power density and electrical efficiency are thus determined by the resistance to oxygen ions across the electrolyte. A higher overall working temperature, or a thinner electrolyte would lower the overall resistance, and hence improve the performance of the unit.

Fig. 3 also displays the electric power density of the unit. It can be seen that the power density initially increases as the current density increases, however since the voltage decreases as the load is increased, and since $P = V\bar{i}''$ the power density reaches a maximum around 7000 A/m^2; above this value performance drops-off. It can also be seen that agreement between the PFM and DNM is quite satisfactory.

3.2. Temperature and current density distributions

Fig. 4 shows iso-values of temperature and current density in the plane of the SOFC electrolyte for a mean current density of $\bar{i}'' = 4000$ A/m^2. A uniform temperature distribution is desirable for a SOFC: Thermally-induced stresses and strains are undesirable as they can lead to cracking of the electrolyte, or failure of the mechanical seals. For the prototype under consideration here, the temperature is a minimum of around 960 K at the air inlet and reaches a maximum value of 1160 K near the air outlet. This temperature distribution is to be expected, since under presumed adiabatic conditions (i.e., well insulated walls) heat can only be removed by bulk convection of the air and fuel. The thermal capacity of air is much larger than for the fuel, so the principle direction of the temperature gradient is primarily aligned with air channels, as shown in Fig. 4.

The maximum temperature value increases as average current density is increased, though not in a linear manner. Heat due to activation increases with current density. Conversely the electrical conductivity of the

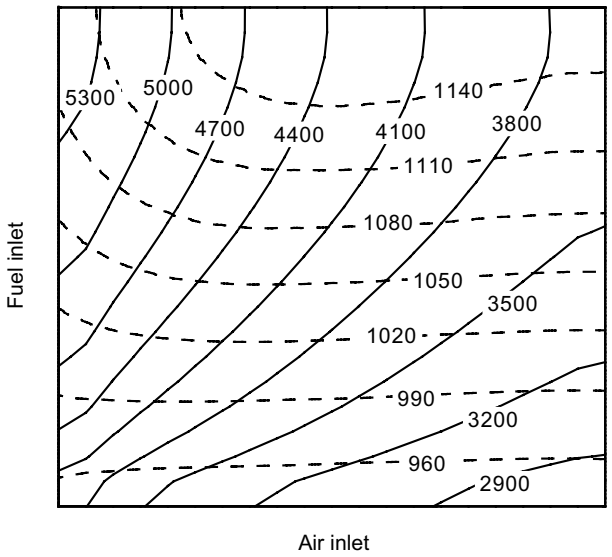

Fig. 4. Electrolyte temperature (°C) (dashed lines) and current density (A/m^2) (solid lines) distributions for the case $\bar{i}'' = 4000$ A/m^2.

electrolyte increases with increasing temperature, as is shown in Fig. 2. Thus the Ohmic resistance decreases and the source due to Joule heating is non-linear. Heat sources associated with the thermodynamics of the electrochemical reactions are by-and-large not a function of current density.

Thermal stresses can cause cracks in the electrolyte. These are more liable to happen if the temperature gradient is large. The variation in temperature gradient is apparent from the spacing of the isothermal lines in Fig. 4. The highest thermal stress occurs in regions where the isothermal lines are most densely populated. The fact that the fuel cell is sandwiched between a pair of thermally-conducting metallic interconnects is highly beneficial. The interconnects act as fins, smoothing out undesirable temperature gradients.

Fig. 4 also shows iso-values of local current density. These vary from a minimum of 2900 A/m^2 to a maximum of more than 5000 A/m^2. It can be seen that the local current density is a maximum at the fuel inlet near the air outlet, and a minimum near the air inlet at the fuel outlet. The location of the maximum coincides with a region where the temperature and mass fraction of H_2 in the fuel is high. The local temperature distribution directly affects the current density distribution since the ionic conductivity of the electrolyte is a strong function of temperature. As the average current density increases, the maximum temperature increases. The temperature gradients are also more significant at higher mean current density values. Temperature is not the only factor which affects the local current density; the Nernst potential decreases as H_2 and O_2 are consumed and H_2O produced, and the local current density also decreases according to Eq. (17).

The impact of the local current density distribution on the performance of a SOFC is significant. Ideally current density would be evenly distributed over the entire electrolyte, in order that the maximum cell voltage is obtained. However, local variation in current density distribution is inevitable in all SOFC designs, and the desired uniformity can never be achieved in practice. Local variation in current density across the electrolyte is one factor which must be considered when evaluating the performance of a SOFC.

3.3. Potential distribution

The local current density and electric potential distributions on the anode-side of a SOFC are shown in Figs. 5 and 6. The anode serves as a diffusion layer for the hydrogen fuel and also the product water. The local current density is obtained as the divergence of the electric field potential for the electronic (and ionic) charge carriers. Analysis of the current density over the solid domain aids in better understanding of the design of SOFCs. For the typical planar SOFC, such as is considered here, neighbouring air/fuel micro-channels are

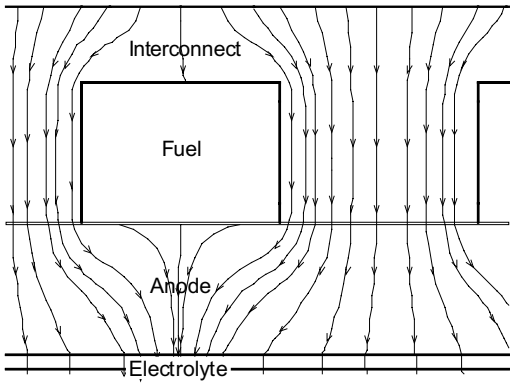

Fig. 5. Current density field around fuel channels.

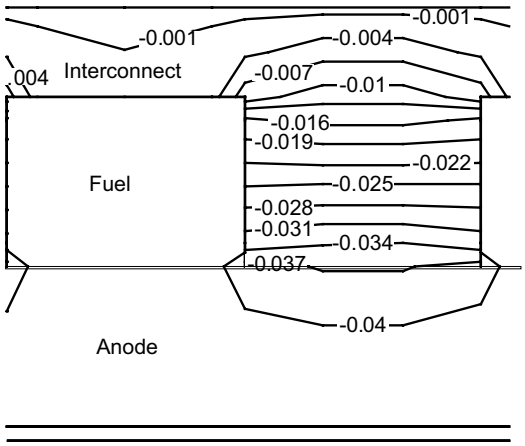

Fig. 6. Electric potential distribution around fuel channels.

separated by solid 'ribs'. Just as the micro-channels provide a path for fluid to diffuse through the pores of the GDLs and reach the catalytic surface at the electrode-electrolyte interfaces; the ribs serve as a means whereby electrons are conducted to the metallic substrate of the porous GDLs, and hence reach the interface sites. At the electrode–electrolyte interface, the current is determined by the gradient of the electric potential, which is a function of the local reactant/product concentration, as well as the local (temperature-dependent) conductance.

Fig. 5 shows flux lines of current density within the fuel-side interconnect. The effect of the rib width on the current density distribution within the interconnect can be seen. At the top plane of the interconnect, local current density values vary due to the rib locations. The electric flux lines are determined entirely by the Laplacian profile associated with the geometry and boundary conditions; however, the latter are themselves a function of the local concentrations of the reactants. These may be non-uniform, especially at high mass transfer rates, when diffusion gradients in the GDL pores are significant. Since mass transfer rates are a function of current density, both geometry and average current density ultimately determine the local potential distribution, which in turn affects the overall performance of the unit. There is a trade-off between the choice of the rib-width (a wide rib would minimise Ohmic resistance) and the need to ensure sufficient mass transfer [15] (a narrow rib will maximise mass transfer in the GDL). The latter is also a function of other variables such as the GDL and micro-channel heights.

Fig. 6 shows the electric field potential around the fuel channels. It can be seen that the iso-potential lines are perpendicular to the fuel channel walls. Higher current densities occur in areas where the iso-potential lines

are more densely distributed. Local current density and electric potential variations affect Ohmic losses in the interconnect, and the resulting Joule heat influences the temperature distribution. The gradient of the electric potential determines the local current density (for constant resistance), and the prediction of potential distribution can provide the following information to the designer: (1) The effect of rib width on current density distribution at the electrolyte interface and on the cell voltage due to Ohmic losses across the interconnects. (2) The effect of the electrode thickness on Nernst potential, and activation overpotentials at the electrolyte interface.

4. Conclusions

The performance of a SOFC depends on the local Ohmic resistance of the electrolyte. This is a function of the temperature distribution and hence the current density (i.e. power dissipation). While evenly distributed temperature and current density distributions are desirable in planar SOFCs; in practice these cannot be attained at present, for a number of reasons.

Comparisons between the detailed-CFD calculations and simpler presumed (inlet) flow approaches suggest simplified methods can, under many circumstances be used to give reliable predictions of the performance of SOFCs as well as detailed CFD methodologies. Comparisons between the results of these two approaches show remarkable similarity in terms of temperature, current density and species mass fraction distributions. Polarisation curves also compare in a favourable manner.

While judicious design of the porous electrodes and electrolyte of a SOFC could greatly improve the electrical performance; other parameters, such as temperature and current density distributions, also play important roles in determining the SOFC performance. Moreover, for the type of anode-supported SOFC considered in the present study, the current density distribution is strongly dependent on the oxygen mass fraction distribution in the cathode.

Predictions of the electric potential distribution made using the detailed CFD code revealed the current flow paths through the bi-polar plates (interconnects) and the electrodes. The electric field potential and current density distribution through these layers affects the rates at which electro-chemical reactions take place, and the overall performance of the SOFC.

References

[1] C. Berger, Handbook of Fuel Cell Technology, Prentice-Hall, England Cliffs, NJ, 1968.
[2] C.G. Vayenas, P.G. Debenedetti, I. Yentekakis, L.L. Hegedus, Cross-flow, solid-state electrochemical reactors: a steady-state analysis, Ind. Eng. Chem. Fundamentals 24 (1985) 316–324.
[3] S.B. Beale, Numerical models for planar solid oxide fuel cells, in: B. Sundén, M. Faghri (Eds.), Transport Phenomena in Fuel Cells, WIT Press, Southampton, 2005.
[4] A. Khaleel, J.R. Selman, Cell, stack and system modelling, in: S. Singhal, K. Kendall (Eds.), High Temperature Solide Oxide Fuel Cells: Fundamentals, Design and Applications, Elsevier, 2003.
[5] S.B. Beale, Y. Lin, S.V. Zhubrin, W. Dong, Computer methods for performance prediction in fuel cells, J. Power Sources 11 (1–2) (2003) 79–85.
[6] S.B. Beale, S.V. Zhubrin, A distributed resistance analogy for solid oxide fuel cells, Numer. Heat Transfer Part B 47 (6) (2005) 573–591.
[7] C.R. Wilke, Diffusional properties of multicomponent gases, Chem. Eng. Progress 46 (2) (1950) 95–104.
[8] A.S. Berman, Laminar flow in channels with porous walls, J. Appl. Phys. 24 (9) (1953) 1232–1235.
[9] J. Jorne, Mass transfer in laminar flow channel with porous wall, J. Electrochem. Soc. 129 (8) (1982) 1727–1733.
[10] S.B. Beale, Calculation procedure for mass transfer in fuel cells, J. Power Sources 128 (2) (2004) 185–192.
[11] R.K. Shah, A.L. London, Laminar flow forced convection in ducts, in: T.F. Irvine, J.P. Hartnett (Eds.), Advances in Heat Transfer, Academic Press, New York, 1978.
[12] P. Costamagna, K. Honegger, J. Electrochem. Soc. 145 (11) (1998) 2712–2718.
[13] S. Nagata, A. Momma, T. Kato, Y. Kasuga, Numerical analysis of output characteristics of tubular SOFC with internal reformer, J. Power Sources 101 (2001) 60–71.
[14] Y. Saad, M.H. Schultz, GMRES: a generalized minimal residual algorithm for solving nonsymmetric linear systems, SIAM J. Scientific Statist. Comput. 7 (3) (1986) 856–869.
[15] J.R. Ferguson, J.M. Fiard, R. Herbin, Three-dimensional numerical simulation for various geometries of solid oxide fuel cells, J. Power Sources 58 (1996) 109–122.